Terr. Atmos. Ocean. Sci., Vol. 20, No. 1, 227-235, February 2009 doi: 10.3319/TAO.2008.01.18.02(F3C)

Observations of the Ionosphere Using the Tiny Ionospheric Photometer

Clayton Coker[1, *], Kenneth F. Dymond[1], Scott A. Budzien[1], Damien H. Chua[1], Jann-Yenq Liu [2], David N. Anderson [3], Sunanda Basu [4], and Todd R. Pedersen [5]

[1] *Space Science Division, Naval Research Laboratory, Washington, District of Columbia, USA*
[2] *Institute of Space Science, National Central University, Chung-Li, Taiwan, ROC*
[3] *University of Colorado/CIRES, NOAA/Space Weather Prediction Center, Boulder, Colorado, USA*
[4] *Center for Space Physics, Boston University, Boston, Massachusetts, USA*
[5] *Air Force Research Laboratory, Space Vehicles Directorate, Hanscom Air Force Base, Massachusetts, USA*

Received 30 May 2007, accepted 18 January 2008

ABSTRACT

The Tiny Ionospheric Photometer (TIP) on the Constellation Observing System for Meteorology, Ionosphere, and Climate (FORMOSAT-3/COSMIC) characterizes the nighttime ionosphere using 135.6-nm radiative recombination emission. TIP measures horizontal structure of the ionosphere with high precision and high spatial resolution. Latitudinal, longitudinal, and temporal distribution of the nighttime ionosphere is specified. We present a review of ionospheric observations made with TIP during the first five months of operation. Comparisons are made with other ionospheric sensors in order to validate the TIP observations and to demonstrate TIP resolution and sensitivity performance. Equatorial anomalies observed by TIP are compared with estimates of the **E B** vertical drift during the post-sunset pre-reversal enhancement in the Peruvian sector. Low latitude irregularity structures observed by TIP are compared with measurements from ground-based sensors including: imaging photometers, ionosonde, and UHF scintillation receivers. Detailed measurements of low latitude density depletion depth and width are provided. Global ionospheric morphology observed by TIP is compared with similar observations by COSMIC radio occultation, and the GAIM model. The complexity of the underlying neutral winds is revealed by the TIP ionospheric morphology.

Key words: Far ultraviolet, Ionosphere, Equatorial anomaly, Irregularities

Citation: Coker, C., K. F. Dymond, S. A. Budzien, D. H. Chua, J. Y. Liu, D. N. Anderson, S. Basu, and T. R. Pedersen, 2009: Observations of the ionosphere using the Tiny Ionospheric Photometer. Terr. Atmos. Ocean. Sci., 20, 227-235, doi: 10.3319/TAO.2008.01.18.02(F3C)

1. INTRODUCTION

The Constellation Observing System for Meteorology, Ionosphere, and Climate (FORMOSAT-3/COSMIC) uses the Tiny Ionospheric Photometer (TIP) to characterize the nighttime ionosphere directly below each spacecraft. TIP is a compact, narrow-band, and ultraviolet photometer operating at the 135.6-nm wavelength (Dymond et al. 2000; Kalmanson et al. 2004). This emission is produced by recombination of O+ ions and electrons, which is the natural decay process for the ionosphere. At night, the strength of the emission is proportional to the square of the electron density integrated over the line of sight (Dymond et al. 1997).

The principal science mission of TIP is to measure the horizontal structure of the nighttime ionosphere. When the horizontal ionospheric structure is measured with sufficient precision, it can be combined with vertical structure measured by GPS radio occultations to reconstruct high accuracy electron density distributions in the ionosphere. TIP is orders of magnitude more sensitive than its FUV predecessors, such as SSULI, LORAAS, SSUSI, GUVI, and IMAGE (Thonnard et al. 1999; Mende et al. 2000; Budzien et al. 2002; Paxton et al. 2003), and provides remarkable detail on ionospheric structures undetected by other FUV sensors. A single TIP pass provides a latitudinal snapshot of the equatorial anomaly and adjacent midlatitude ionospheres with 15 - 30 km spatial resolution, depending on the altitude of the satellite. A sequence of passes maps the latitudinal and longitudinal distribution of the ionosphere at a given local time. Once the satellites are distributed into separate orbital planes, the combined TIP passes will moni-

* *Corresponding author*
E-mail: clayton.coker@nrl.navy.mil

tor the horizontal distribution of the ionosphere at several local times. This provides for the specification and study of the temporal evolution of the ionosphere.

This paper describes some of the ionospheric observations made with TIP during the first five months of operation. During this period the relative sensitivity between TIP sensors and flight module number five (FM5) was estimated by comparing sensors in the same orbital plane. FM1, FM3, and FM6 data were adjusted to match the sensitivity of FM5 by multiplying by the following factors, 1.1, 1.2, and 0.7, respectively. A 135.6-nm detector sensitivity of 600 counts s^{-1} Rayleighs^{-1} was used during this period. This sensitivity is similar to the sensitivity reported by Dymond et al. (2009), derived from comparisons with incoherent scatter radar and radio occultation data. Section 2 of this paper describes observations of the equatorial anomaly in the Peruvian sector and compares these with measurements of **E B** vertical drift at the magnetic equator. Section 3 describes observations of low latitude irregularities and compares these with ground-based sensors. Section 4 focuses on the global morphology of the low latitude ionosphere and compares TIP with other global data sets.

2. EQUATORIAL ANOMALY

One of the most important features of TIP is the ability to observe the equatorial anomaly. A TIP pass over the anomaly region observes primarily the latitudinal structure of the anomaly. At the equator, 40 of latitude is sampled in about 10-min. Since the orbital inclination of the COSMIC satellites is 72 , this same 10-min pass also traverses about 10 in longitude.

Figure 1 shows examples of the equatorial anomaly observed by TIP over the Peruvian sector shortly after sunset (1900 - 2100 LT). At this time of day the peak density of the anomaly crests is driven by the pre-reversal enhancement in the **E B** drift at the equator (Farley et al. 1986; Whalen 2004). Figure 1a shows the TIP observed anomaly as a function of magnetic latitude in the Peruvian sector for day 256 (13 September 2006). TIP shows two well-formed crests at 12 geomagnetic latitude, with a slight asymmetry favoring the southern crest. The anomaly trough (near the magnetic equator) is deep and shows evidence of structuring, coincident with bottom-side spread F observed by the digisonde at Jicamarca, Peru. One hour earlier, the vertical plasma **E B** drift at the equator was estimated to be 22 m s^{-1}, using changes in the height of the layer as measure by the digisonde at Jicamarca (Bertoni et al. 2006). A vertical drift of 22 m s^{-1} confirms the well formed anomaly observed by TIP. Figure 1b shows an overall weaker post-sunset anomaly on 28 May, which is confirmed by a weaker vertical drift of 10 m s^{-1} measured an hour earlier by the digisonde at Jicamarca. The average crest magnitude is used when comparing with the vertical drift estimate of the pre-reversal enhancement. And finally, Fig. 1c shows that when the post-sunset pre-reversal enhancement is absent (0 m s^{-1} vertical drift), no anomaly crests are formed. These results show that the TIP observations of the post-sunset equatorial anomaly track the strength of the pre-reversal enhancement.

3. LOW LATITUDE IRREGULARITIES

Another important feature of TIP is the ability to observe low latitude depletions and bubbles and the ionospheric context in which they form and evolve. TIP provides sufficient resolution and sensitivity to observe these structures even during solar minimum, when the ionospheric densities are low. From the parking altitude of 500 km, TIP observes a 15-km spot in the F-region ionosphere. From the operational altitude of 800 km, the spot in the F-region is 30 km. TIP data is generally integrated over a 1-s period. During this time the ionospheric spot moves about 7 km, due to the satellite motion. Thus, the data provides adequate spatial resolution to observe low latitude irregularity structures. With sensitivities in the hundreds of counts s^{-1} Rayleigh^{-1}, even relatively weak low latitude structures are observed at solar minimum.

Figure 2 shows the TIP data for 14 September 2006, at an altitude of 500 km over the western half of the Pacific Ocean from flight modules FM1, FM3, and FM6. These spacecraft were in the same orbital plane, so they sample very similar local times. Together they provide a regional picture of the ionosphere near 2100 LT. TIP sensitivity to visible light is observed on passes over the dense urban areas of Japan, but does not affect the data over oceans and rural areas. On this night, the low latitude ionosphere was much more developed over the central Pacific Ocean than the

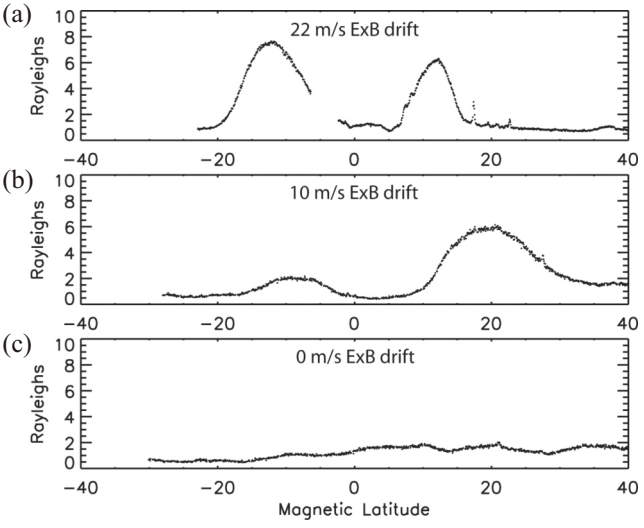

Fig. 1. TIP observations of the post-sunset, equatorial anomaly over the Peruvian sector on (a) 13 September 2006, (b) 28 May 2006, and (c) 26 May 2006.

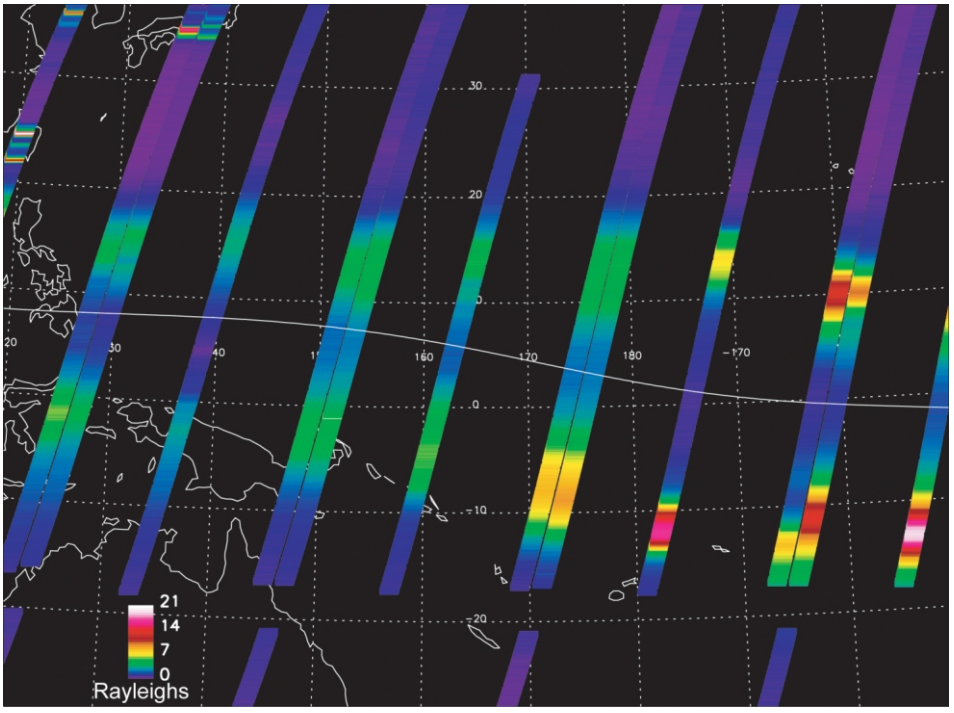

Fig. 2. Map of ionosphere over the western Pacific Ocean on 14 September 2006 using 135.6-nm radiances from FM1, FM3, and FM6 near 2100 LT at equator.

Guam sector. This is observed by comparing the intensity of the 135.6-nm emission and the separation of the anomaly crests. Brighter crests and wider crest separation implies a stronger post-sunset pre-reversal enhancement. Instabilities reaching the higher density anomaly crests are anticipated to produce larger scintillation effects.

In addition to the large scale (~4000 km) longitudinal variability in the post-sunset anomaly, the data in the Hawaiian sector shows tremendous variability from one pass to the next. Figure 3a shows the TIP data for this sector as a function of magnetic latitude. Even though the tracks of FM6 and FM3 are separated by only 200 km in longitude, the anomaly crests vary by nearly a factor of 2. Furthermore, the northern crest of the FM6 pass and the southern crest of the FM3 pass show strikingly similar features. Each shows a significantly reduced crest magnitude with a depletion along the equatorward wall. Optical data from Hawaii, southward directed and narrow field 630.0-nm data (not shown), confirms the presence of two depletion structures at this time separated by about 500 km. This implies that the TIP observed variation in the crests is primarily due to irregularity formation and, by comparing adjacent crest samples between FM6 and FM3, the breadth and magnitude of the depletions are clearly observed against the background ionosphere. TIP travels along the depletions for about 6 and 9 of magnetic latitude for FM6 and FM3, respectively. Given the orbital inclination of the satellites and the orientation of the magnetic field lines, this implies that the depletions are 100 and 160 km wide in longitude, respectively. The magnitudes of the depletions are about 30% and 80% of the background radiance, respectively, when compared to the adjacent anomaly crest. The third pass, FM1, is about 1400 km west of the first two passes and also shows evidence of structuring.

Figure 3b shows the TIP data over the Kwajalein sector. FM6 and FM3 pass east of Kwajalein about 1000 km, whereas, FM1 passes about 300 km west of Kwajalein. The ionosphere is much quieter in this sector, but still shows some evidence for minor low latitude irregularities. FM6 and FM3 show remarkably similar anomalies. These are significantly less bright than those in the adjacent sector and show moderate asymmetry favoring the southern crest. The anomaly under FM1 is even dimmer still, but shows evidence of a depletion or two on the equatorward wall of the northern crest. This is consistent with observations of spread F on the digisonde at Kwajalein and with moderate VHF scintillation observed from Kwajalein, which start around 0900 UT and continue for several hours.

Figure 3c shows the TIP data over the Guam sector. The post-sunset ionosphere is even weaker here than over the Kwajalein sector, but still shows evidence of minor structuring on the southern crest of the FM1 pass over western New Guinea. This is confirmed by the presence of moderate VHF scintillation, which was observed along a fixed line of site east of Guam for only an hour starting around 1230 UT. Note at the equator the deeper trough in the FM1 pass com-

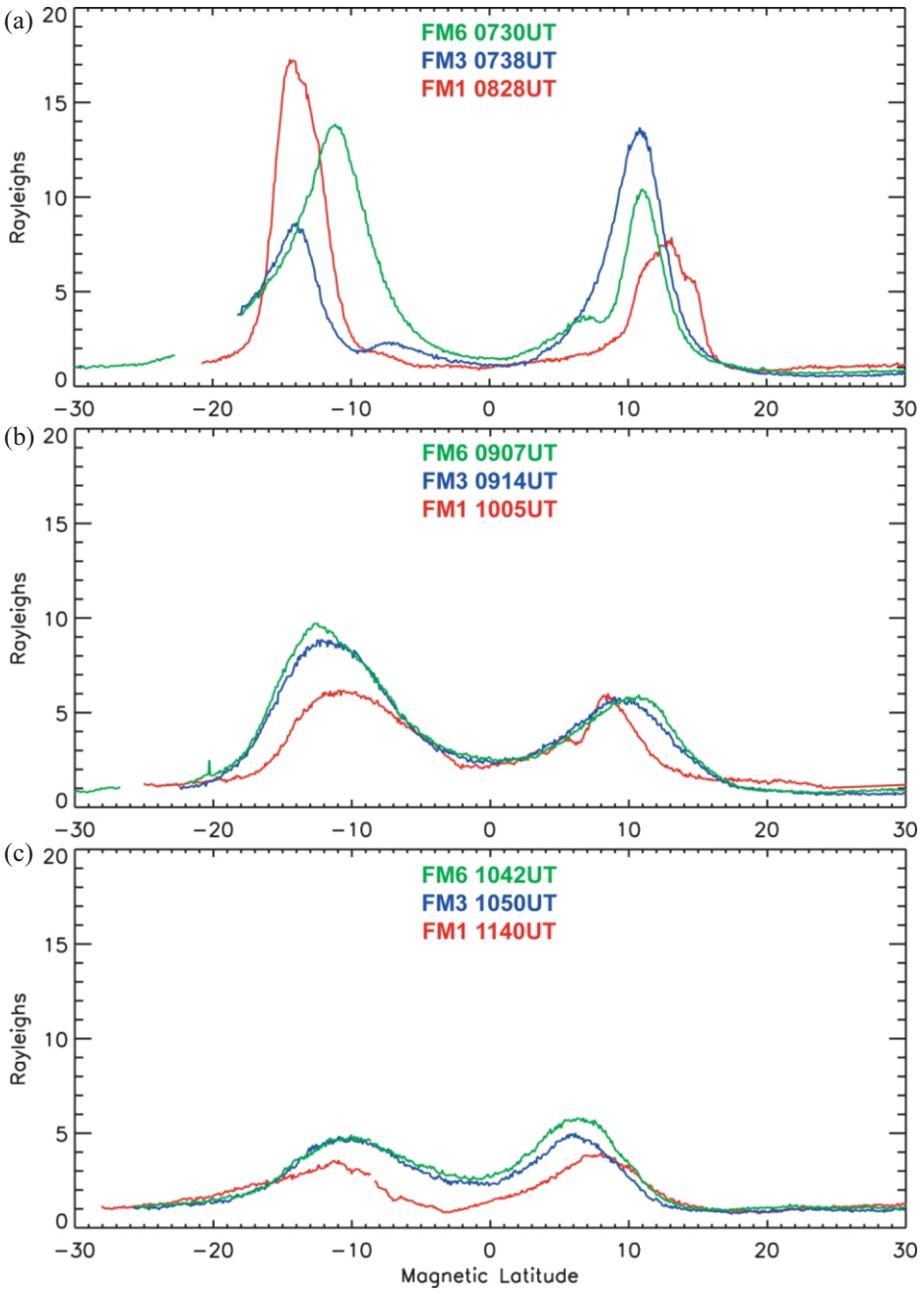

Fig. 3. TIP passes over the western Pacific Ocean on 14 September 2006 from FM1, FM3, and FM6 over the (a) Hawaiian sector, (b) Kwajalein sector, and (c) Guam sector.

pared to the FM3 pass and the FM6 pass, all at 500 km altitude. This is either an indicator of enhanced vertical drift or the presence of a depletion at the equator. The regional map of TIP data for 14 September (see Fig. 2) clearly shows the variation of the anomaly as a function of longitude and sectors where the potential for scintillation is greater, but most of the detailed structuring can only be observed using the line plots (ssee Fig. 3). By comparing the structured samples with estimates of the background ionosphere, quantitative estimates of the depletion structures can be produced.

TIP data over the Kwajalein sector was also compared with the 630.0-nm data from the allsky camera on Roi Namur. Figure 4a displays the TIP FM5 pass over the sector on 17 September 2006 and shows an oddly shaped anomaly. The sharply peaked northern crest, broad trough, and suppressed southern crest are similar to the features observed earlier on 14 September over the Hawaiian sector (see Fig. 3a). These features are indicators of irregularity structuring. Figure 4b displays the track of FM5 superimposed over the allsky 630.0-nm image, projected to a 300-km altitude. The

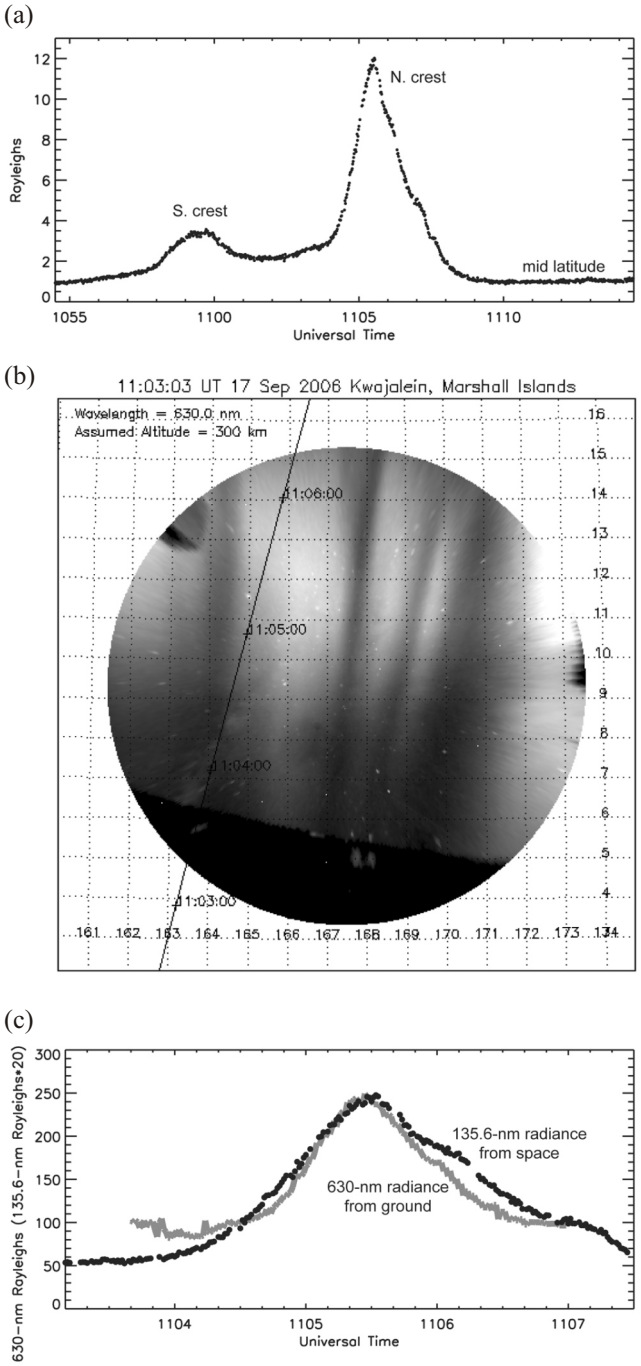

Fig. 4. TIP and allsky imager observations of low latitude structure over Kwajalein on 17 September 2006: (a) TIP FM5 135.6-nm observation of anomaly in Kwajalein sector, (b) 630.0-nm allsky image projected to 300 km altitude and track of FM5, and (c) comparison of TIP 135.6-nm data and allsky 630.0-nm data along the track of FM5.

allsky image shows a series of depletions against the backdrop of the northern anomaly crest. FM5 begins its journey across the imager field of view in a depletion and diagonally crosses the anomaly crest before entering the next depletion poleward of the crest. This path through the area is what produces the features observed on FM5. In order to verify this, the 630.0-nm data along the FM5 trajectory were extracted from the image and compared with the TIP data (see Fig. 4c). The ground-based 630.0-nm data and the space-based 135.6-nm data agree remarkably well. Both show a similar slope and peak of the anomaly crest, including the undulating poleward slope. The 630.0-nm data has a background limited sensitivity of about 100 Rayleighs, so the fact that TIP shows emissions below this level is not a problem. It merely demonstrates that TIP is more sensitive than the allsky camera. Overall the comparison reveals that TIP observes the anomaly and irregularity structures with a high degree of sensitivity and resolution.

4. GLOBAL MORPHOLOGY

Previously, passes from a few TIP sensors in the same local time frame were used to display a regional map of the equatorial anomaly and reveal its longitudinal variation. The global variability of the anomaly at a given local time can be observed by projecting 24 h of TIP data onto a map. Figure 5a shows the global longitudinal morphology of the anomaly near 2100 LT 14 September 2006. The post-sunset anomaly shows longitudinal enhancements and decreases and latitudinal asymmetries. These reveal the complexity of low latitude ionospheric drivers, namely, the meridional and zonal neutral winds, and the resulting electric field at the magnetic equator. The anomaly is enhanced in four sectors of the globe, specifically the African, Indonesian, central Pacific, and South American sectors. Between these sectors the anomaly weakens in the western and eastern Pacific sectors and completely collapses in Indian and Atlantic sectors. This global pattern is remarkably similar to observations made by the IMAGE FUV sensor at equinox and attributed to atmospheric tides (Immel et al. 2006). These so-called 4-cell patterns of non-migrating tides, which arise from tropospheric weather, drive thermospheric winds, which in turn drive the equatorial anomaly.

Figure 5b shows the global 2100 LT ionosphere specified by the Global Assimilation of Ionospheric Measurements (GAIM) model using GPS ground stations, ionosondes, and topside electron density sensors for 14 September 2006. Vertical 135.6-nm emission was estimated from GAIM using simple radiative recombination rate at 1160 K (Meléndez-Alvira et al. 1999) without neutralization and scattering terms (Dymond et al. 1997). GAIM 135.6-nm emission shows a similar 4-cell pattern of enhancements in the anomaly, with clear enhancements over African, Indonesian, and South American sectors. GAIM shows just a hint of the enhancement over the central Pacific sector, but this is not surprising, since ground-based data is sparse over large ocean areas and the underlying climatology may not capture the 4-cell pattern very well. GAIM agrees with TIP in the Atlantic sector, showing the collapse of the anomaly, but does not show a similar collapse, merely a decrease,

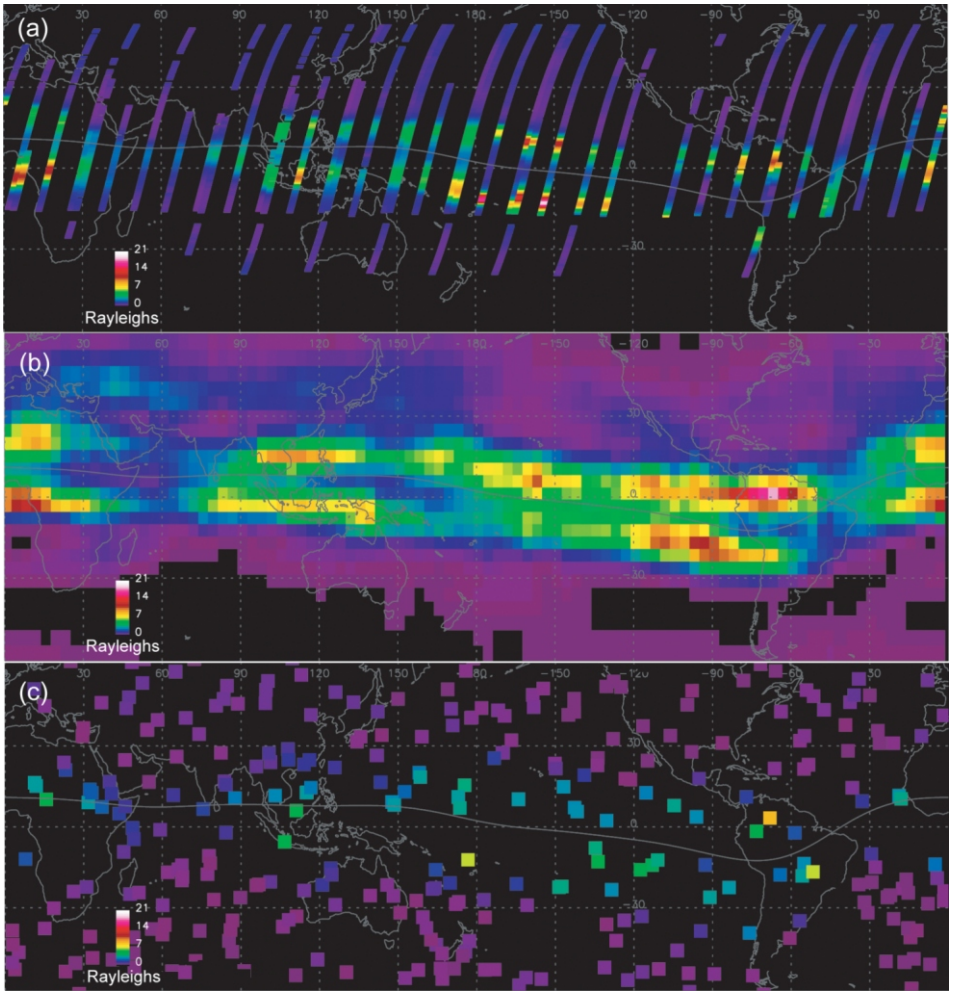

Fig. 5. Global maps of 2100 LT ionosphere on 14 September 2006 from: (a) 135.6-nm radiance from TIP sensors on FM1, FM3, and FM6, (b) 135.6-nm radiance from GAIM model, and (c) 135.6-nm radiance from radio occultations from FM1, FM3, FM4, and FM6.

in the anomaly magnitude over the Indian sector. This discrepancy is attributed to the sparsity of ground-based data in the region and the underlying climatology. Over the South American and African continents, where ground-based GPS is more readily available, the agreement is quite good. GAIM does not have the spatial resolution or underlying physics to model irregularity features. This can be seen in the African sector, where a single TIP pass reveals a dramatic density depletion along the pass in the northern anomaly crest just west of the Greenwich meridian.

Figure 5c shows the global 2100LT ionosphere specified by radio occultations from four COSMIC spacecraft in the same orbital plane: FM1, FM3, FM4, and FM6. Occultations were restricted to be within 45 azimuth from the orbit trajectory. The resulting Abel inverted electron density profiles and estimated vertical 135.6-nm radiances are within 50 min local time of the TIP observations. The radio occultation and TIP data show some similar global ionospheric features. Radio occultations show the collapse of the equatorial anomaly over the Indian and Atlantic sectors and they show that no collapse occurs over the Pacific Ocean. However, the more subtle pattern of enhancements and decreases over the Pacific Ocean are not observed in the radio occultation data. Furthermore, the radio occultations do not clearly reveal individual features of the anomaly. The crests and trough are not clearly defined as they are with TIP or even the GAIM model, which has a low horizontal resolution similar to the Abel inversions. This is not a terribly surprising result, considering that the Abel inversion assumes spherical symmetry in the ionosphere on the order of 2000 km. Non-linear horizontal gradients in the ionospheric density or changes in the height of the layer over this distance cause the Abel inversion to mischaracterize the peak density and shape of the layer. In the vicinity of the equatorial anomaly, the inversion tends to underestimate the density profile at the anomaly crests and overestimate the density profile in the trough and transitions from low to mid-latitudes. In order to demonstrate this more clearly, Fig. 6 shows a comparison of the TIP data and radio occultation data as a function of magnetic latitude. One day of TIP data

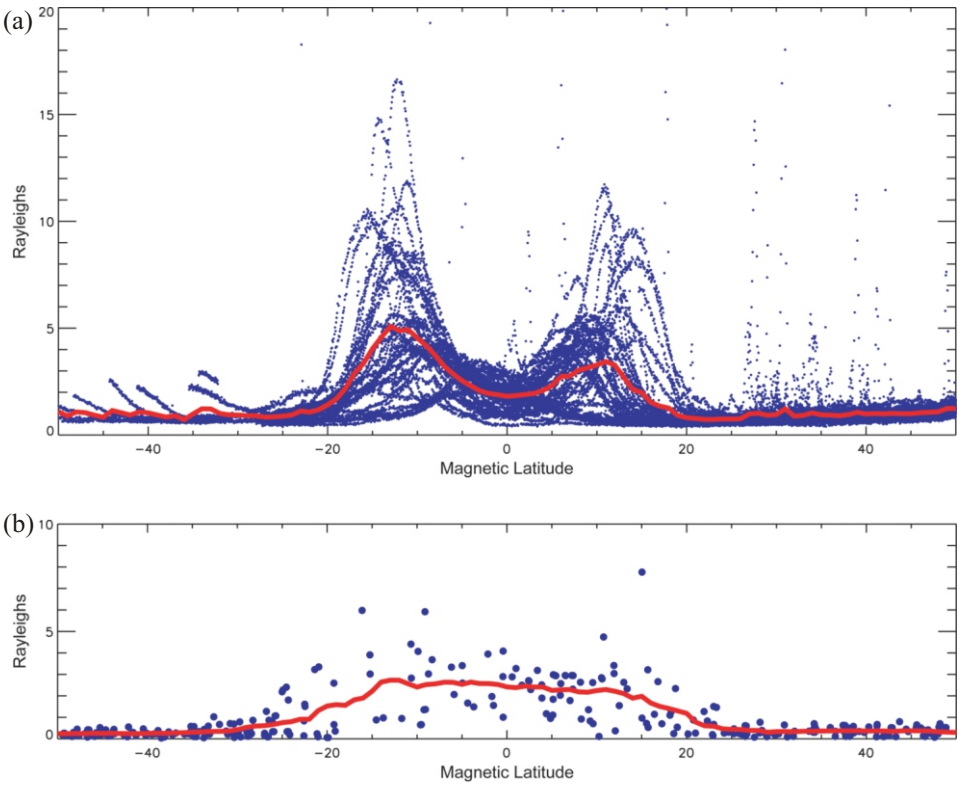

Fig. 6. Comparison of global ionospheric data on 14 September 2006 as a function of magnetic latitude from: (a) TIP sensor date and average and (b) radio occultations and average with magnetic latitude.

from three spacecraft in the same orbit show tremendous longitudinal variability and high resolution latitudinal details of the equatorial anomaly. The data also show two noise issues: effects of the South Atlantic Anomaly appear as ramps in the southern latitudes below 30 S; and the sensitivity to visible light appears as spikes, when TIP passes over urban areas at mostly northern latitudes. An average of the TIP data with magnetic latitude shows the mean global anomaly for 2100 LT 14 September 2006, with average crest locations at 12 magnetic latitude and an asymmetry that favors the southern crest. The radio occultation data show little evidence of any features of the anomaly. The average of the radio occultation data shows a broad equatorial mound with no evidence of an anomaly trough or crests. Comparing the TIP and radio occultation averages indicates that the Abel inversions underestimate the crests and overestimate the trough and transitions from low to midlatitudes. It can be argued that a single day of radio occultations does not provide a sufficient sampling of the global equatorial anomaly, and this may account for some of the differences between the TIP and radio occultation data. Multiple days of radio occultations would provide improved sampling of the global equatorial anomaly and may help to confirm these observations.

The comparison between TIP and radio occultation data helps explain earlier radio occultation validation results against ionosondes (Jakowski et al. 2005). Here, occultations near southern Europe systematically overestimated the density profile; whereas, occultations near northern Europe did not. Occultations from the transition zone between low and midlatitudes may have biased the comparisons with southern European ionosonde stations.

This potential trouble spot for Abel inversions also shows up in the estimation of ionospheric peak height, hmax. At the transition from low to midlatitudes, the Abel inversions can produce artificially low peak heights. This can be seen in Fig. 7, where post-sunset, peak heights resulting from Abel inversions on 14 September 2006 are plotted as a function of magnetic latitude. The average peak height is also shown. The average TIP 135.6-nm radiance is superimposed on the figure in order to show the location of the global, post-sunset anomaly. In the transitions from low to mid latitudes, the peak heights are frequently lower than expected. Here the ionosphere at the tangent point is relatively weak compared to the adjacent poleward edge of the post-sunset anomaly crest. Slant TEC values through the crest are comparable to TEC values at the tangent point. This causes a broadening of the TEC profile and the Abel inverted density profile, especially on the bottomside. Thus the height of the peak density is artificially low in these cases. This observation helps explain earlier radio occultation validation results, where statistical comparisons with globally distributed iono-

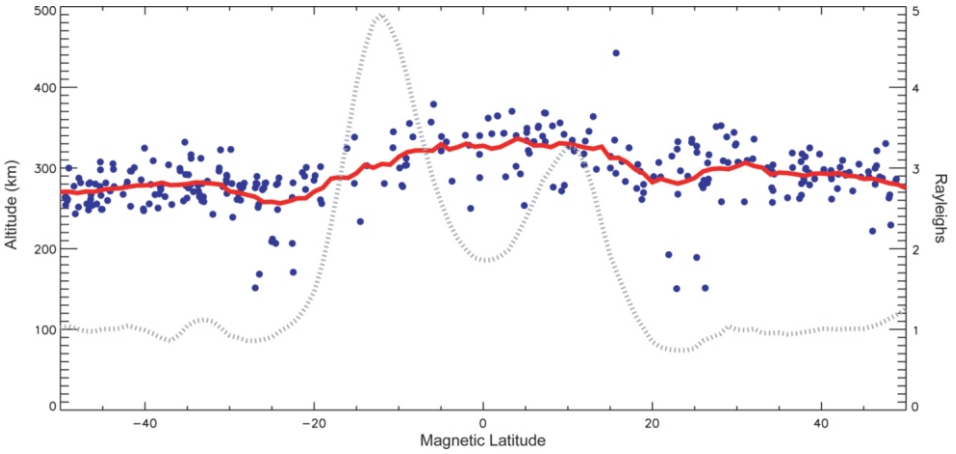

Fig. 7. Radio occultation ionospheric peak heights from 14 September 2006 as a function of magnetic latitude, (solid line) average peak height, and (dotted line) average TIP radiance showing location of anomaly features.

sondes showed a systematic negative bias in the occultation-derived peak height (Jakowski et al. 2002).

At midlatitudes, TIP 135.6-nm radiances are systematically higher than the radio occultation-derived radiances by a fraction of a Rayleigh (Fig. 6). Here the Abel inversions are less prone to error, since there are fewer horizontal gradients. This systematic difference has a couple of possible explanations. First, background emissions from long wavelength light may bias the TIP data. While the TIP detector is optimized for FUV light, it has some residual sensitivity to longer wavelengths. At 250 nm the detector sensitivity is down by three orders of magnitude. The Herzberg oxygen bands (250 - 400 nm), which have been estimated to emit 225 Rayleighs at night (Meier 1991), could produce a background emission of a few tenths (20 - 30%) of a Rayleigh in the TIP data, which accounts for the systematic difference.

Second, other factors affecting 135.6-nm emission may account for the low level differences between TIP observed radiances and the radio occultation-derived radiances. These factors include electron temperature dependence, charge neutrality assumption, neutralization and scattering (Dymond et al. 1997). Initial modeling of these terms suggest that neutralization may be able to account for the differences between TIP and radio occultations at midlatitudes. At solar minimum the ionosphere is lower in altitude, which enhances the neutralization term. However, the magnitude of this effect is not firmly established.

Whatever the source of this error, comparisons with midlatitude radio occultation data can be used to monitor it. Similarly, comparisons with low latitude radio occultation data and their Abel inversions can be used to calibrate the sensitivity of the TIP sensors, if a sufficient number of samples are obtained. Dymond et al. (2009), described another calibration technique, which uses radio occultation data. This approach combines an in-plane occultation with TIP data over the low latitude region, and performs a 2D reconstruction of the electron density (Dymond and Thomas 2001). The sensitivity of the TIP detector and the bias of the radio occultation total electron data are output from this process.

5. SUMMARY

TIP reveals the latitudinal morphology of the nighttime equatorial anomaly with each pass over the low latitude region. TIP observations of the magnitude of the anomaly crests tracked estimates of the maximum value of the pre-reversal enhancement in the post-sunset, Peruvian sector. The magnitude of the crests, their relative asymmetry, and location provide insight into the zonal and meridional winds, which drive the latitudinal morphology.

TIP provides ample sensitivity and spatial resolution to observe low latitude irregularity structures, even during solar minimum. Depletions in plasma density were observed over the Pacific Ocean and confirmed by independent observations using ground-based sensors, including imagers, UHF scintillation monitors, and an ionosonde. Interpretation of these depletions is sometimes complicated by the fact that TIP samples the depletions primarily in latitude rather than longitude. Adjacent TIP passes were used to specify the background ionosphere and provide a clear picture of the magnitude and width of the depletions. Direct comparison between TIP and the allsky imager at Kwajalein was used to validate TIP observations of the anomaly crest and adjacent depletions.

Global comparison of TIP data with radio occultation data were made and serve to validate the TIP data and reveal a possible calibration technique. This comparison suggests limitations of the Abel inversions at low latitudes. The radio occultations appear to under estimate electron densities in the crests of the anomaly and over estimate the density in the trough and transitions from low to midlatitudes. At midlatitudes the comparison revealed a low level (~0.4 Rayleighs) bias) bias in the TIP data, attributed to long wavelength

emissions or possible mismodeling of the 135.6-nm volume emission rate. The comparisons with GAIM validated the global morphology of the equatorial anomaly observed by TIP and revealed limitations of the data coverage and underlying Climatology used by the model. TIP provides sufficient sensitivity to observe the global ionospheric morphology during solar minimum, when the ionosphere is weak. This morphology reveals the complexity of the zonal and meridional neutral winds, which drive the post-sunset equatorial anomaly. The morphology observed at equinox showed a pattern of anomaly enhancements and decreases consistent with the non-migrating tide 4-cell pattern, which arises from tropospheric weather patterns. TIP promises to be a valuable asset for further investigations into atmosphere-ionosphere coupling, the formation of the nighttime equatorial anomaly, and the development of low latitude irregularities.

Acknowledgements This work was supported by the US Office of Naval Research.

REFERENCES

Bertoni, F., I. S. Batista, M. A. Abdu, B. W. Reinisch, and E. A. Kherani, 2006: A comparison of ionospheric vertical drift velocities measured by digisonde and incoherent scatter radar at the magnetic equator. *J. Atmos. Sol.-Terr. Phys*., **68**, 669-678, doi: 10.1016/j.jastp.2006.01.002. [Link]

Budzien, S. A., K. F. Dymond, S. E. Thonnard, A. C. Nicholas, D. M. Diez, and R. P. McCoy, 2002: On-orbit characterization and performance of the HIRAAS instruments aboard ARGOS: LORAAS sensor performance. In: Larar, A. M. And M. G. Mlynczak (Eds.), Optical Spectroscopic Techniques, Remote Sensing, and Instrumentation for Atmospheric and Space Research IV, *Proc. SPIE*, **4485**, 349-360, doi: 10.1117/12.454269. [Link]

Dymond, K. F. and R. J. Thomas, 2001: An algorithm for inferring the two-dimensional structure of the nighttime ionosphere from radiative recombination measurements. *Radio Sci.*, **36**, 1241-1254, doi: 10.1029/2000RS002429 [Link].

Dymond, K. F., S. E. Thonnard, R. P. McCoy, and R. J. Thomas, 1997: An optical remote sensing technique for determining nighttime F region electron density. *Radio Sci.*, **32**, 1985-1996.

Dymond, K. F., J. B. Nee, and R. J. Thomas, 2000: The tiny ionospheric photometer: An instrument for measuring ionospheric gradients for the COSMIC constellation. *Terr. Atmos. Ocean. Sci.*, **11**, 273-290.

Dymond, K. F., S. A. Budzien, D. H. Chua, C. Coker, and J. Y. Liu, 2009: Tomographic reconstruction of the low-latitude nighttime electron density using FORMOSAT-3/COMSIC radio occultation and UV photometer data. *Terr. Atmos. Ocean. Sci*., **20**, 215-226, doi: 10.3319/TAO.2008.01.15.01(F3C). [Link]

Farley, D. T., E. Bonelli, B. G. Fejer, and M. F. Larson, 1986: The prereversal enhancement of the zonal electric field in the equatorial ionosphere. *J. Geophys. Res.* **91**, 13723-13728, doi: 10.1029/JA091iA12p13723. [Link]

Immel, T. J., E. Sagawa, S. L. England, S. B. Henderson, M. E. Hagan, S. B. Mende, H. U. Frey, C. M. Swenson, and L. J. Paxton, 2006: Control of equatorial ionospheric morphology by atmospheric tides. *Geophys. Res. Lett*., **33**, L15108, doi: 10.1029/2006GL026161. [Link]

Jakowski, N., A. Wehrenpfennig, S. Heise, C. Reigber, H. Lühr, L. Grunwaldt, and T. K. Meehan, 2002: GPS radio occultation measurements of the ionosphere from CHAMP: Early results. *Geophys. Res. Lett.*, **29** , 1457, doi: 10.1029/2001GL014364. [Link]

Jakowski, N., K. Tsybulya, J. Mielich, A. Belehaki, D. Altadill, J. C. Jodogne, and B. Zolesi, 2005: Validation of GPS radio occultation measurements on CHAMP by vertical sounding observations in Europe. In: Reigber, C., H. Lühr, P. Schwintzer, and J. Wickert (Eds.), Earth Observation with CHAMP, Results from Three Years in Orbit, Springer-Verlag Berlin, 447-452.

Kalmanson, P. C., S. A. Budzien, C. Coker, and K. F. Dymond, 2004: The tiny ionospheric photometer instrument design and operation. In: Nardell, C. A., P. G. Lucey, J. H. Yee, and J. B. Garvin (Eds.), Instruments, Science, and Methods for Geospace and Planetary Remote Sensing, *Proc. SPIE*, **5660**, Bellingham, WA, doi: 10.1117/12.578341. [Link]

Meier, R. R. , 1991: Ultraviolet spectroscopy and remote sensing of the upper atmosphere. *Space Sci. Rev.*, **58**, 1-185, doi: 10.1007/BF01206000. [Link]

Meléndez-Alvira, D. J., R. R. Meier, J. M. Picone, P. D. Feldman, and B. M. McLaughlin, 1999: Analysis of the oxygen nightglow measured by the hopkins ultraviolet telescope: Implications for ionospheric partial radiative recombination rate coefficients. *J. Geophys. Res*., **104**, 14901-14913, doi: 10.1029/1999JA900136. [Link]

Mende, S. B., H. Heetderks, H. U. Frey, M. Lampton, S. P. Geller, S. Habraken, E. Renotte, C. Jamar, P. Rochus, J. Spann, S. A. Fuselier, J. C. Gerard, R. Gladstone, S. Murphree, and L. Cogger, 2000: Far ultraviolet imaging from the IMAGE spacecraft: 1 system design. *Space Sci. Rev.*, **91**, 243-270, doi: 10.1023/A:1005271728567. [Link]

Paxton, L. J., D. Morrison, D. J. Strickland, M. G. McHarg, Y. Zhang, B. Wolven, H. Kil, G. Crowley, A. B. Christensen, and C. I. Meng, 2003: The use of far ultraviolet remote sensing to monitor space weather. *Adv. Space Res.*, **31**, 813-818, doi: 10.1016/S0273-1177(02)00886-4. [Link]

Thonnard, S. E., S. A. Budzien, A. C. Nicholas, K. F. Dymond, and D. P. Drob, 1999: An update on the calibration and performance of the Special Sensor Ultraviolet Limb Imagers (SSULI). In: Carruthers, G. R. and K. F. Dymond (Eds.), Ultraviolet Atmospheric and Space Remote Sensing: Methods and Instrumentation II, *Proc. SPIE*, **3818**, doi: 10.1117/12.364145. [Link]

Whalen, J. A., 2004: Linear dependence of the postsunset equatorial anomaly electron density on solar flux and its relation to the maximum prereversal $\mathbf{E} \times \mathbf{B}$ drift velocity through its dependence on solar flux. *J. Geophys. Res*., **109**, A07309, doi: 10.1029/2004JA010528. [Link]